Activated nano-Al_2O_3 loaded on polyurethane foam as a potential carrier for fluorine removal

Zhe Wang [a], Xinyue Gu [a], Yufeng Zhang [a], Xinbo Zhang [a,*], Huu Hao Ngo [a,b,**], Yang Liu [a], Weibing Jiang [a], Xinai Tan [c], Xiao Wang [d], Jianqing Zhang [d]

[a] *Joint Research Center for Protective Infrastructure Technology and Environmental Green Bioprocess, School of Environmental and Municipal Engineering, Tianjin Chengjian University, Tianjin 300384, PR China*
[b] *Centre for Technology in Water and Wastewater, School of Civil and Environmental Engineering, University of Technology Sydney, Sydney, NSW 2007, Australia*
[c] *Dayu environmental protection Co., Ltd, Tianjin 301739, PR China*
[d] *TG Hilyte Environment Technology (Beijing) Co., LTD., Beijing 100000, PR China*

* Corresponding author.
** Correspondence to: H.H. Ngo, Joint Research Center for Protective Infrastructure Technology and Environmental Green Bioprocess, School of Environmental and Municipal Engineering, Tianjin Chengjian University, Tianjin 300384, PR China.
E-mail addresses: zxbcj2006@126.com (X. Zhang), ngohuuhao121@gmail.com (H.H. Ngo).

Keywords:
Polyurethane foam
Activated nano-
Al2O3 Adsorption
Fluorine removal

A B S T R A C T

Fluorine is an essential trace element for human beings and animals and it helps to build strong bones and teeth. It is, however, also toxic to biological health in that an excessive intake of fluorine concentration from a water environment could be dangerous. This study aims to develop a novel and recoverable composite foam polyurethane foam (PUF)-Al_2O_3 for fluorine removal. The proposed material was developed using dopamine hydrochloride as the underwater adhesive connecting with the adsorption function group of activated nano-Al_2O_3 and PUF. The activated nano-Al_2O_3 in the PUF was characterized by SEM and XRD, and the results indicated that PUF-Al_2O_3 surface hydrophilicity rose significantly when compared with the original PUF. The foam PUF-Al_2O_3 steadily removed fluorine with a maximum adsorption capacity of 2.08 mg/g. The adsorption isotherm of PUF-Al_2O_3 was fitted well to the Langmuir isotherm model while the pseudo-first-order model well described the adsorption kinetics of PUF-Al_2O_3. The composite foam reached adsorption equilibrium in a relatively short time of approximately 10 min. The PUF-Al_2O_3 presented an excellent regeneration performance in 10 mg/L fluorine solution after 5 cycles. Further adsorption mechanism analysis indicated the ion exchange mechanism played a decisive role in PUF-Al_2O_3 foam's fluorine removal.

1. Introduction

Fluorine is now widespread in many counties of the groundwater bodies and it is traceable to natural and human factors [1,2]. Fluorine migrates to water because of physical and chemical action when groundwater flows through rocks rich in fluorine. Fluoride contaminant is generated from not only the scour of geological but also a large amount of fluoride industrial wastewater discharge. These include but are not limited to glass ceramics, semiconductor manufacturing, electroplating, aluminum smelting, brick-making, steel, thermal power generation and other industries. These all produce huge amounts of fluoride wastewater which increase the likelihood of large-scale fluoride pollution. Fluorine is an essential trace element for human beings and animals and it helps to build strong bones and teeth, but also has toxic characteristics which can endanger biological health [3]. An excessive intake of fluorine ion concentration from a water environment is harmful to people. Excessive fluoride intake leads to dental fluorosis, bone disease, disruption of phosphorus metabolism, stunted growth in children, and even an increased risk of cancer, such as of the bladder, uterine, and colon.

Many countries around the world were suffering the dangers of ingesting excessive fluorine ion bring. Word Health Organization (WHO) stipulated that the standard of drinking water beneficial amount of fluoride ion is less than 1.5 mg/L. Some countries have regulated there must be no more than 1.0 mg/L [4,5]. The fluoride removal from drinking water remains as the issue of considerable attention. Up to now, traditional technologies regularly employed to remove fluorine include membrane technologies [6,7], ion-exchange [8,9], coagular

precipitation [10] and adsorption [11–13]. Although these technologies' effectiveness in removing fluorine has been confirmed, they do have some shortcomings. For example, membrane fouling may occur when membrane materials are utilized for too long, leading to rising maintenance costs. Ion-exchange is susceptible to interfering ions, efficiency greatly depends on PH, and other media after multiple reuse create toxic substances.

Adsorption is the simplest water treatment process and superior to convenient operations, due to its low cost, high selectivity, and reuse of adsorbent. Employing an adsorbent is essential for fluoride removal and various types of adsorbent materials have been used for it. These include chitosan, activated carbon fiber, pulverized fuel ash, bentonite, zeolite, etc. [13–18]. The activated nano-Al_2O_3 has outstanding fluoride removal properties due to its large specific surface and high mass transfer efficiency [19–21]. However, activated nano-Al_2O_3 usually has a small size and is difficult to recycle after adsorption, which will lead to secondary pollution.

In order to address the problem of activated nano-Al_2O_3 recycling difficulty, this study adopts the immobilization method to fix the activated nano-Al_2O_3 on the carrier surface and interior. When the carrier is immersed in the fluorine solution to be treated, the reaction between fluoride ion and the activated nano-Al_2O_3 can help achieve removal. It is convenient to carrier regeneration and recycling. Polyurethane foam (PUF) open cell with a polyether group is suitable as a substrate for adsorbent materials because it has excellent mechanical strength, good water stability, and flexible structure, which can effectively prevent secondary pollution and contribute to recycling for the purposes of reuse [22,23]. However, how to endow the PUF with adsorptive properties for fluorine removal is crucial. Dopamine (DOPA) has powerful wet adhesion capacity and currently has great potential in the design of adhesives' applications [24]. Therefore, in order to improve the adsorbent removal fluoride ion capacity and regenerability, prevent secondary pollution caused by adsorbent particles, we introduced the activated nano-Al_2O_3 materials and employed dopamine hydrochloride as the underwater adhesive synergistic activated nano-Al_2O_3 loaded on PUF open cell foam to prepare the PUF composition for the research of water depth defluoridation. This preparation process will give the new matrix a much improved fluorine removal ability and maintain the PUF advantage of convective transport. The new PUF composite adsorbent was characterized in detail to analyze its morphology and microstructure. Furthermore, the fluoride ion adsorption properties of PUF composite material were systematically investigated.

2. Materials and methods

2.1. Primary materials

The PUF sample for this study was supplied by Shandong Yi-Nuo Polyurethane Co., Ltd., China. The PUF contained polyether. Trimethylaminomethane, polyethyleneimine (PEI) and dopamine hydrochloride were purchased from Sigma-Aldrich. DI water was produced by Millipore Milli-Q Advantage A10 (Billerica, MA, USA). The activated nano-Al_2O_3 was obtained from Shanghai Macklin Biochemical Co., Ltd., China. All the other chemicals were of analytical purity.

2.2. Synthesis of the PUF-Al_2O_3 composite foam

The process of synthesizing PUF-Al_2O_3 composite foam was done according to previous research [25]. Typically, 0.3 g Trimethylaminomethane was dissolved in 250 mL DI water and adjusted pH = 8.5 with 0.2 mol/L HCl, 0.5 g dopamine hydrochloride and 0.5 g activated nano-Al_2O_3 were added to obtain the 10 mM Tris-dopamine buffered solution. The PUF was dipped into a 4 g/L PEI water solution for 1 h to improve the hydrophilic and wet performance of foam. Following this the PUF was cleaned three times using deionized water and transferred to the Tris-dopamine buffered solution for stirring which lasted 4 h to form the PUF-Al_2O_3 composite foam.

2.3. Characterization of PUF-Al_2O_3 composite foam

The surface morphology of PUF-Al_2O_3 composite foam was examined by scanning electron microscope (SEM, Hitachi S-4800, Japan). The composite foams phase was measured by X-ray diffractograms (XRD, Bruker, D8 Advance, USA). N_2 adsorption/desorption measurements were conducted at 77 K (Quanta chrome, ASIQ, USA). The BJH pore size-distribution was calculated by the Kelvin equation. The foams were cut into pieces and degassed at 100 °C under vacuum at less than 1×10^{-5} bar for 6 h prior analysis. The water contact angle (WCA) of PUF-Al_2O_3 composite foam surface was examined on a Krüss Instrument (CM3250-DS3210, Germany) at ambient temperature. X-ray photoelectron spectroscopy (XPS) served to determine the surface elemental composition of the samples with a Quanta 200 spectrometer (FEI Co., Ltd., USA) with a monochromatic Al Ka X-ray source (1486.6 eV photons) at a pass energy of 93.9 eV. The fluoride ion concentration was measured by ion chromatograph (Dionex Aquion).

2.4. Fluoride ion adsorption experiments

The fluoride ion adsorption performance of the PUF-Al_2O_3 composite foam was evaluated through a static adsorption experiment of adsorption isotherm and kinetics. The PUF-Al_2O_3 composite foam was put into a plastic tube containing NaF solution at a specific concentration. Following this the tube was oscillated through the incubator shaker at an ambient temperature. The adsorption solution was withdrawn at predetermined intervals to measure the fluoride ion concentration, in order to establish what the kinetic adsorption was. The uptake capacity (mg/g) was calculated as follows:

$$q = (c_0 - c_e)V/m \quad (1)$$

where c_0 and c_e, respectively, are the incipient and adsorption equilibrium fluoride ion concentration (mg/L), V is the solution volume (L), and m is the mass of PUF-Al_2O_3 composite foam (g).

The aluminum sulfate solution desorbed the fluoride ion from PUF-Al_2O_3 composite foam. The composite foam was put into a plastic tube with the concentration of 10 mg/L fluoride ion solution to be shaken and adsorbed for 1 h. Subsequently, the previously prepared 10% aluminum sulfate solution served to desorb the saturated composite foam for 30 min. Finally, the composite foam was withdrawn and washed by DI water. Repeating the above steps led to acquiring and calculating the regeneration efficiency (RE) of the composite foam according to the following formula (2):

$$RE = q_2/q_1 * 100\% \quad (2)$$

where q_1 and q_2 are, respectively, the uptake of the first use and repeated use.

3. Results and discussion

3.1. Foam surface morphology and physical structure analysis

The SEM images of PUF and PUF-Al_2O_3 composite foam at different magnifications and EDS analysis result are shown in Fig. 1. Clearly observed here is the interconnected open cell foam construction in the image of PUF (Fig. 1 a). Furthermore the smooth porous wall was observed at a higher magnification micrograph (Fig. 1 b, c). The PUF-Al_2O_3 composite foam still retained the open cell structure compared with the PUF (Fig. 1 e). However, a large activated nano-Al_2O_3 emerged and loaded on the composite foam surface at a higher magnification micrograph (Fig. 1 f, g). The EDS analysis result indicated that the element of Al obviously emerged after anchoring the activated nano-Al_2O_3 in the foam (Fig. 1 d, h). This was made possible by the strong

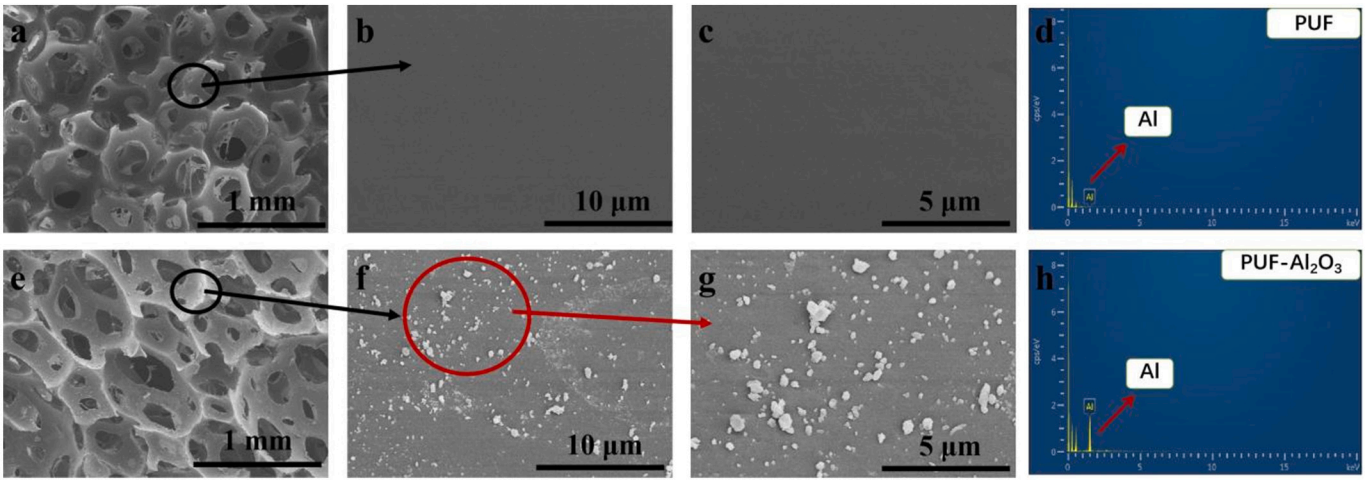

Fig. 1. The foam surface SEM images and EDS analysis: PUF (a, b, c, d), PUF-Al_2O_3 composite foam (e, f, g, h).

adhesion ability of dopamine immobilized onto the foam surface through the coagulation solution. Anchoring the nanoparticles of Al_2O_3 endowed the foam with functional properties. Indicated here was that the activated nano-Al_2O_3 was successfully loaded into the open cell PUF.

The XRD pattern of PUF and PUF-Al_2O_3 was measured and the results are depicted in Fig. 2. It is observed that the diffraction peaks of Al_2O_3 at 2θ positions 27.22°, 35.22°, 38.10°, 39.95°, 42.65°, 54.48°, 55.92°, 59.47°, and 67.53° matched well with the (102), (103), (112), (004), (202), (212), (204), (231) and (220) lattice planes, respectively [26,27]. These positions of the diffraction peak corresponded to the Al_2O_3 standard card (JCPDS No. 26-0031). The diffraction peak at 2θ position 19.96° presented an amorphous form of the PUF. The above results simultaneously indicated nanoparticles of Al_2O_3 were loaded in the PU foam.

The N_2 adsorption-desorption isotherm and BJH adsorption pore size distribution of PUF-Al_2O_3 are both illustrated in Fig. 3. As shown in Fig. 3A, the isotherm curve was type IV with a H3 hysteresis loop. It indicated that the PUF-Al_2O_3 had a mesoporous structure and the slit-shaped pores are evident in the amorphous porous layered of Al_2O_3 [20,28,29]. The pore size distribution curve of the desorption branch is shown in Fig. 3B, which reveals the peak primary located at 2.8 nm and the distribution range was up to 34 nm. It is suggested here that: firstly, the PUF-Al_2O_3 was mainly composed of mesopore structure; secondly, this pore size was larger than the diameter of fluoride ion (0.133 nm); and thirdly, the fluoride ion could pass into the pore of activated nano-Al_2O_3 [21]. The specific surface area of PUF-Al_2O_3 was 11.51 m^2/g, which was higher than the original PUF (0.32 m^2/g) and this was attributed to the added activated nano-Al_2O_3 which increased the specific surface area.

3.2. Foam surface wettability

The hydrophilicity of pristine PUF and PUF-Al_2O_3 composite foam was studied by measuring the water contact angle. As shown in Fig. 4 (A_1 and A_2), the pristine foam surface revealed intense hydrophobicity and the contact angle was maintained in 110.3 ± 0.81 at 60 s. This was due to the pristine PUF having a large number of tiny pores and relatively hydrophobic surface of polyether PUF, which hindered the solution's permeability with the compact construction of foam. The foam was immersed in PEI water solution with the hydrophilic group of -NH_2 in order to improve the foam surface's hydrophilicity and wettability [30]. This process and the desired outcome indicated that the PUF-Al_2O_3 composite foam surface contact angle changed to 96.1 ± 1.10 after 60 s (Fig. 4 B_1 and B_2). Furthermore the hydrophilicity increased significantly compared with pristine PUF. Dopamine hydrochloride covered in the PUF not only had strong adhesion capacity to immobilize Al_2O_3 nanoparticles, it also enhanced the wettability with the group of -OH and -NH_2. The PEI infiltration and dopamine hydrochloride coating helped the surface to transform from a hydrophobic to hydrophilic character, and further enhanced water penetration.

3.3. Effects of fluorine concentration on the adsorption

As an important indicator of adsorption properties, the influence of

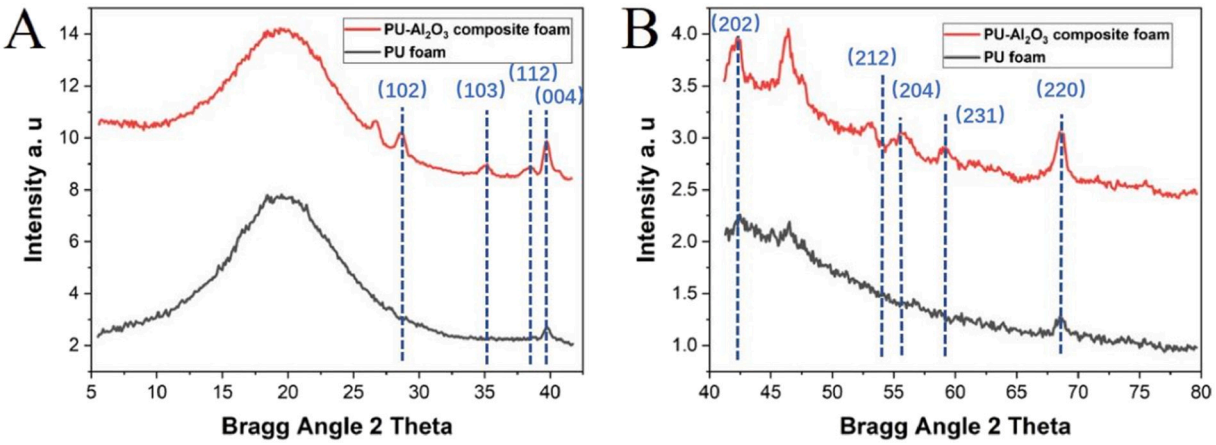

Fig. 2. The phase structure of PUF and PUF-Al_2O_3 with XRD patterns.

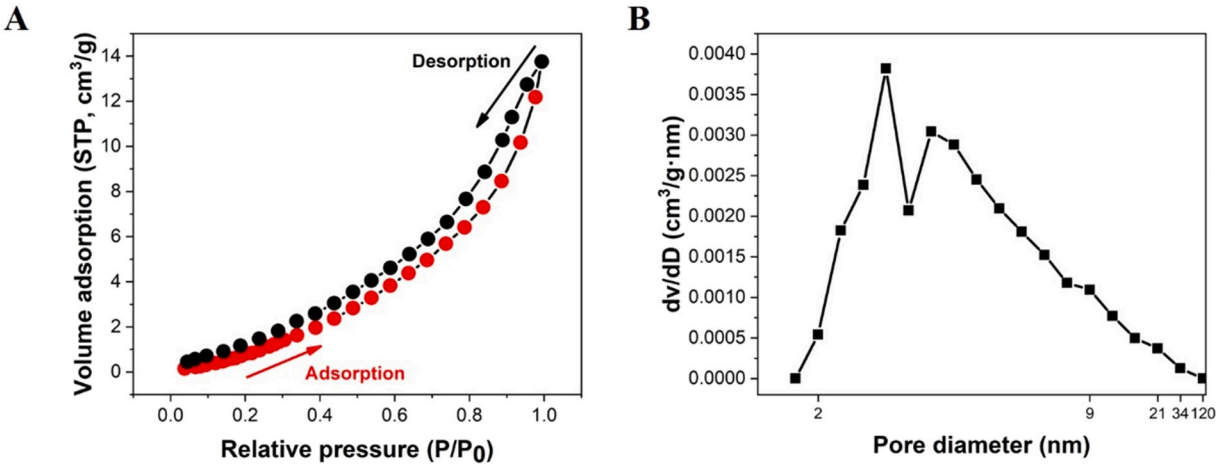

Fig. 3. N_2 adsorption/desorption isotherms (A) and pore size distributions of PUF-Al_2O_3 (B).

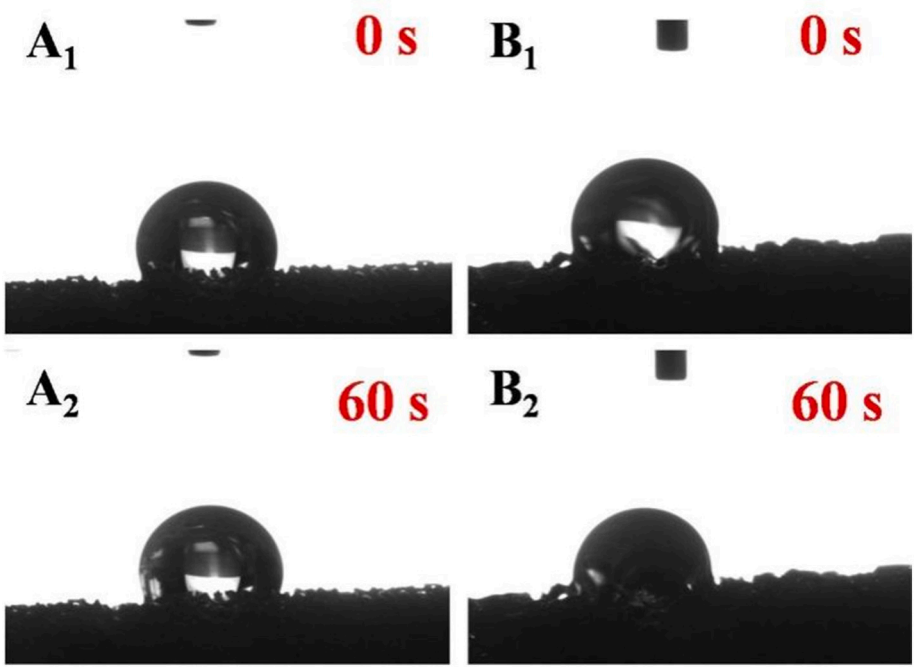

Fig. 4. The WCA evolution of foam surface from 0 to 60 s. (A_1 and A_2 are pristine foam, B_1 and B_2 are PUF-Al_2O_3 composite foam).

different initial fluoride ion concentrations was investigated for PUF-Al_2O_3 open cell composite foam. The fluoride ion uptakes of composite foam are 0.48 mg/g, 0.77 mg/g, 1.88 mg/g, 2.05 mg/g, 2.08 mg/g and 2.10 mg/g when the initial fluorine concentration are, respectively, 5.84 mg/L, 12.01 mg/L, 24.00 mg/L, 45.99 mg/L, 75.35 mg/L and 93.78 mg/L. This indicated that the fluoride ion adsorption capacity of PUF-Al_2O_3 composite foam increased with the initial fluoride ion concentration. Interestingly, the fluoride ion uptake quickly increased at the beginning, and subsequently the adsorption capacity stabilized when the initial fluorine concentration of solution exceeded 50 mg/L and the maximum adsorption capacity was 2.08 mg/g. It is strongly suggested that the PUF-Al_2O_3 composite foam exists in the form of activated nano-Al_2O_3, leading to a steady diffusion rate and negated the influence of rising concentration gradient. This benefited the adsorption of fluorine ions at a smaller concentration [30]. Meanwhile, the activated nano-Al_2O_3 when put into the PUF not only improved diffusion and adsorption capacity, but also prevented the active nanoparticles being separated from PUF during adsorption.

3.4. Adsorption isotherm

The adsorption isotherm of PUF-Al_2O_3 composite foam was researched by plotting the fitted curve for further analysis of the adsorption process. Both Langmuir and Freundlich adsorption isotherm models were referred to in order to explain the experimental data. The Langmuir and Freundlich models follow Eqs. (3) and (4), respectively [31], which are written below:

$$q = \frac{q_{\max} b c_{eq}}{1 + b c_{eq}} \tag{3}$$

$$q = K_f c_{eq}^{1/n} \tag{4}$$

where q is the fluoride ion uptake according to experimental (mg/g) at equilibrium concentration, c_{eq} is the concentration at equilibrium (mg/L), q_{max} is the maximum fluoride ion adsorption capacity (mg/g), and b is the sorption coefficient of Langmuir (L/mg). Furthermore k_f and 1/n, respectively, are the constant and heterogeneity coefficient of the

Freundlich isotherm.

The fitted curve and parameters are shown in Fig. 5 and Table 1. Indicated here is that the Langmuir isotherm model has a higher value of R^2, which better described the PUF-Al_2O_3 composite foam's adsorption behavior. This outcome revealed the Langmuir isotherm as a monolayer adsorption process was only connected with the adsorption sites of activated nano-Al_2O_3 and fluoride ion interaction, strongly suggesting that the adsorption energy is constant.

The pH effect is an important part of the adsorption process, and it can determine the fluoride ion adsorption capacity of PUF-Al_2O_3 composite foam. Experimental results found that the values of pH were 5.8 and 6.2 before and after adsorption, respectively. It revealed that the variable pH quantity changed only very little. Studies showed that the best possible adsorption capacity of Al_2O_3 was present when the pH ranged between 5.4 and 6.5 [20,32]. A mass of hydrogen ions triggers the desorption process in a too low pH environment. Moreover, the negative ions competing with fluoride ion in alkaline state reduced the adsorption capacity.

3.5. Adsorption kinetics

Fig. 6 shows the adsorption kinetics of PUF-Al_2O_3 composite foam with 20 mg/L initial fluoride ion concentration. It is observed that the composite foam quickly reached adsorption equilibrium in approximately 10 min. These results were encouraging and indicated the PUF-Al_2O_3 composite foam reached the adsorption equilibrium in a relatively short time, and achieved a higher efficiency adsorption rate. It therefore has commercial application value. The rapid efficient adsorption could be due to abundant active sites of activated nano-Al_2O_3 being dispersed and exposed on the PUF surface. It was more likely to access fluoride ion to complete the adsorption process. To determine the adsorption mechanisms of the PUF-Al_2O_3, four classical kinetic models, namely the pseudo-first-order (PFO) [33], pseudo-second-order (PSO) [34], intraparticle diffusion [30] and Elovich [35] were used to analyze the contact time and fluoride ion uptake. The equations are written as follows (Eqs. (5)–(8)):

$$\text{PFO}: ln\ (q_e - q_t) = ln\ q_e - k_1 t \quad (5)$$

$$\text{PSO}: t/q_t = 1/k_2 q_e^{\,2} + t/qe \quad (6)$$

$$\text{Intraparticle diffusion}: q_t = k_p\ t^{1/2} \quad (7)$$

$$\text{Elovich}: q_t = 1/\beta\ ln\ (1 + \alpha\beta t) \quad (8)$$

where q_e and q_t are respectively the adsorption uptake at time (t) min and equilibrium, k_1 (min^{-1}) and k_2 (min^{-1}), respectively, are the rate constants of adsorption of the PFO and PSO, k_p (mg (g $min^{1/2})^{-1}$) is the intraparticle diffusion rate constant. Meanwhile α and β are the initial adsorption rate (g mg−1 min−1) since dqt/dt → α, qt → 0 and constant of desorption (g mg^{-1}), the Elovich's equation can be assumed that βt > > 1. In this way the equation becomes $q_t = 1/\beta \ln(\alpha\beta) + (1/\beta) \ln t$ [36].

Table 1.
The list of isotherm parameters for fluorine removal using PUF-Al_2O_3composite foam.

	Langmuir constants			Freundlich constants		
PUF-Al_2O_3 composite foam	q_{max}	b	R^2	K_f	1/n	R^2
	2.599	0.06	0.95	0.32	0.43	0.86

The plot fit of the four kinetic models is shown in Fig. 6 and the correlative regression coefficients of each model are listed in Table 2. It is evident that the PFO predicted the kinetics behavior of PUF-Al_2O_3 composite foam very well due to the higher correlation coefficient. It emerged that the PFO was the most suitable model for describing the kinetics process. As well, the kinetics behavior suggested that the adsorption process of the PUF-Al_2O_3 composite foam occurred mainly through chemisorption because the hydroxyl ion existing on the surface and interior of activated nano-Al_2O_3 triggered ion exchange reaction with fluoride ion. Moreover, there are fairly strong and simultaneous electrostatic attractions and hydrogen bonds [37].

3.6. Regeneration of PUF-Al_2O_3 composite foam

The regeneration performance of PUF-Al_2O_3 composite foam was researched to evaluate the adsorbent from an economic perspective. The adsorption-desorption outcome of PUF-Al_2O_3 composite foam with 10 mg/L fluorine solution is depicted. It emerged that the fluorine ion adsorption capacity of PUF-Al_2O_3 does not significantly change when the cycle number increases. This finding indicated that the dopamine hydrochloride as the underwater adhesive strongly anchored the activated nano-Al_2O_3 on the PUF and guaranteed the nanoparticles did not fall off after 5 cycles. Subsequently, the regeneration revealed the PUF-Al_2O_3 composite foam has a high and stable recycling performance.

3.7. Adsorption mechanism

In order to further explore the adsorption mechanism of PUF-Al_2O_3 adsorption fluoride ion, the chemical state and composition were analyzed by XPS. The spectra of PUF-Al_2O_3 before and after adsorption are shown in Fig. 7. It can be seen from the XPS wide scans spectra (Fig. 7 A_1 and B_1) that a new F 1s species spectra appeared by comparison after

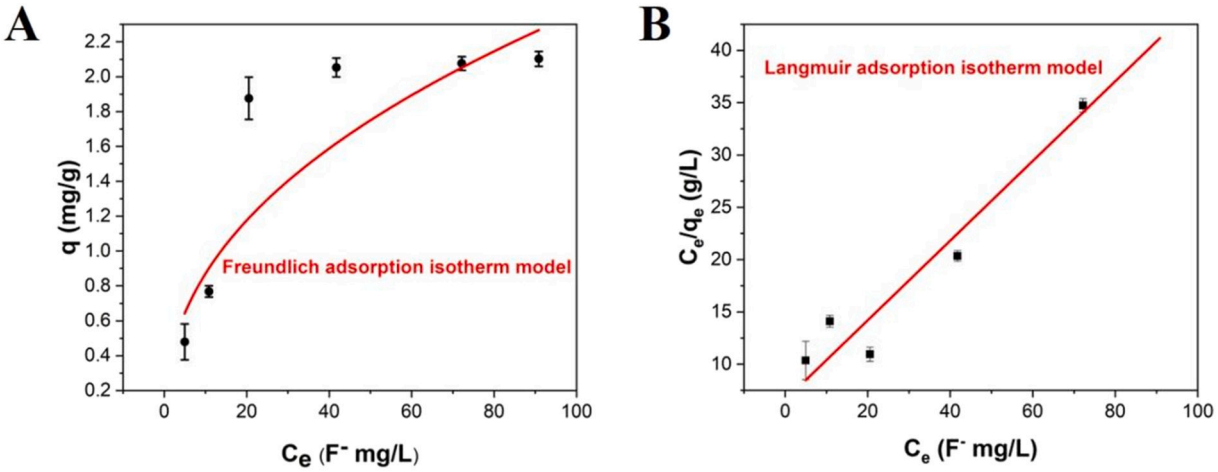

Fig. 5. The equilibrium concentration adsorption effect and adsorption isotherms of PUF-Al_2O_3 composite foam (A: Freundlich isotherm, B: Langmuir isotherm).

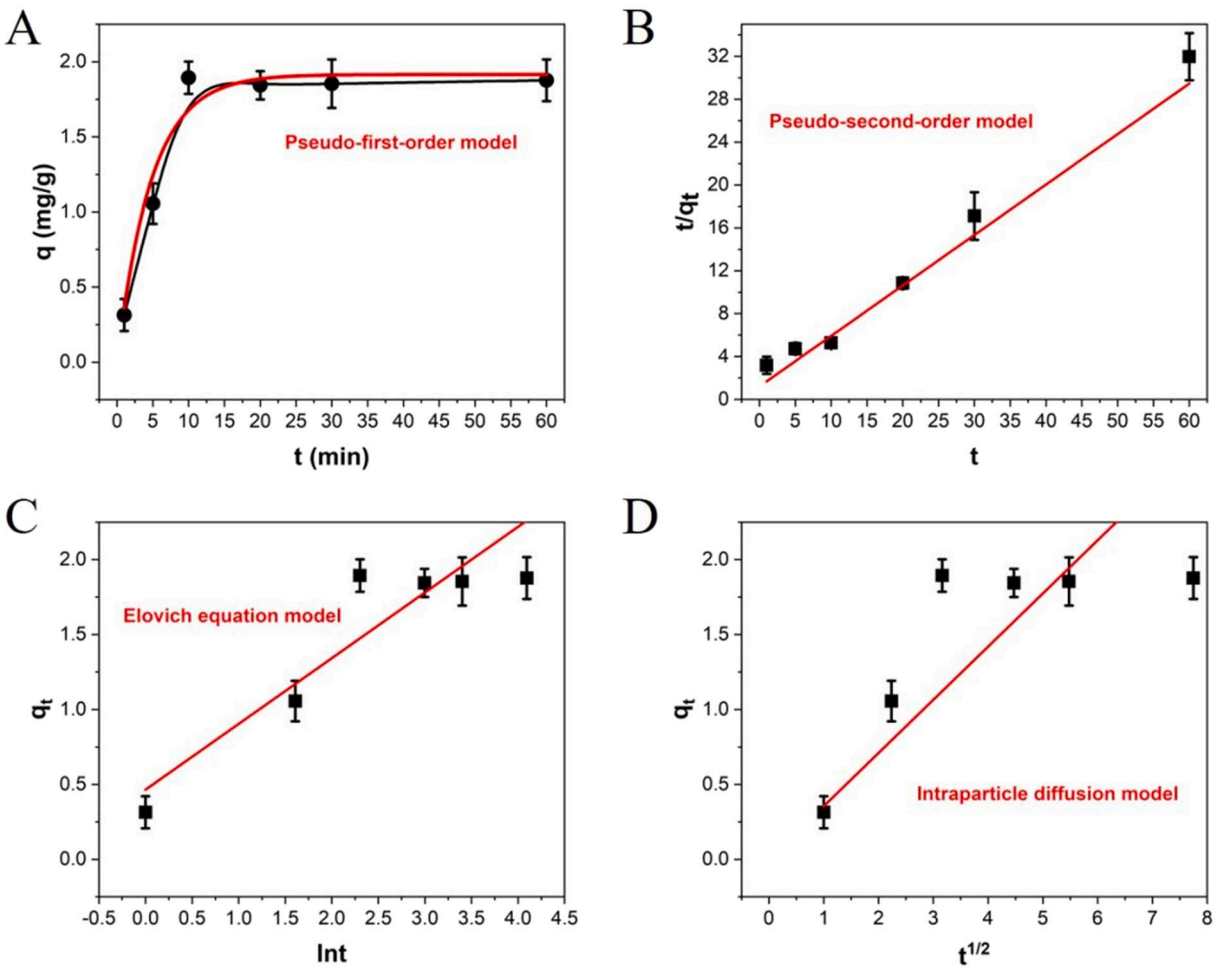

Fig. 6. The kinetics of PUF-Al_2O_3 composite foam at fluoride ion concentration of 20 mg/L and the kinetics fitted curve (A: PFO, B: PSO, C: Elovich, D: Intra-particle diffusion).

Table 2
PUF-Al_2O_3composite foam adsorption kinetic parameters.

	Pseudo-first-order			Pseudo-second-order			Elovich			Intraparticle diffusion	
PUF-Al_2O_3 composite foam	q_e	k_1	R^2	q_e	k_2	R^2	α	β	R^2	K_p	R^2
	1.91	0.21	0.95	2.12	0.18	0.93	1.27	2.28	0.81	0.36	0.89

PUF-Al_2O_3 adsorption fluoride ion. This indicated that the adsorbent material wields an obvious adsorption effect on fluoride. Peak components for O 1s in the spectra are analyzed and the 'before' and 'after' adsorption results are shown in Fig. 7 A_2 and B_2. According to the binding energy of O 1s spectra are attributable to Al—O and Al—OH species in 530.8 and 532.1 eV [38]. It can be seen that the Al-OH peak percentage decreased from 64.04% to 57.93%, while the ratio of Al—O increased from 35.96% to 42.07%. The diminished Al-OH species peak percentage proves that the –OH plays an important role in the process of fluoride ion adsorption, which occurred largely via ion exchange reaction with hydroxyl groups replaced by fluoride ion. The results of Al 2p spectra peaks are shown in Fig. 7 A_3 and B_3. It can be seen that the Al 2p spectra main emission peaks variation trend of Al-OH and Al—O according to the results of O 1s spectra [27]. As well, two new peaks appear after adsorption at 76.5 and 75.4 eV and this can be attributed to the AlF_3 and $AlF_{2.7}(OH)_{0.3}$ species, respectively [39,40]. The $AlF_{2.7}(OH)_{0.3}$ species served as the intermediate of the adsorption reaction. Meanwhile the corresponding composition of PUF-Al_2O_3 before and after adsorption is listed in Table 3, and the element percentage variations are noted here.

The adsorption mechanism of PUF-Al_2O_3 composite foam can be further described. In this research, the PUF only as the adsorbent carrier and the activated nano-Al_2O_3 play a decisive role in the adsorption process. The composite foam adsorbed fluorine ions were mainly attributed to tripartite aspects. Firstly, the surface of activated nano-Al_2O_3 adhered much of the hydroxy group at the weak acid solution system (the pH value was more than 5.0), which leads to the ion exchange reaction, as shown in the reaction (9) [41]. Additionally, the fluorine ion has stronger electronegative attraction and this helped to form a hydrogen bond with the hydroxy group, when using Eq. (10). Secondly, the hydroxy group on the activated nano-Al_2O_3 surface was prone to protonation which helped to obtain -OH_2^+ in an acidic solution (when the pH value was less than 5.0) [37]. The activated nano-Al_2O_3 surface is positively charged and this highlighted the role of electrostatic attraction and ligand exchange mechanism. The correlation reaction process is documented below in Eq. (11) to (13). Thirdly, the complexation reacted to the activated nano-Al_2O_3 internal and external surfaces with fluorine ion [42]. Based on the above XPS analysis and adsorption mechanism discussion, the main mechanism of the PUF-Al_2O_3 composite foam is ion exchange. This is due to the pH ranging

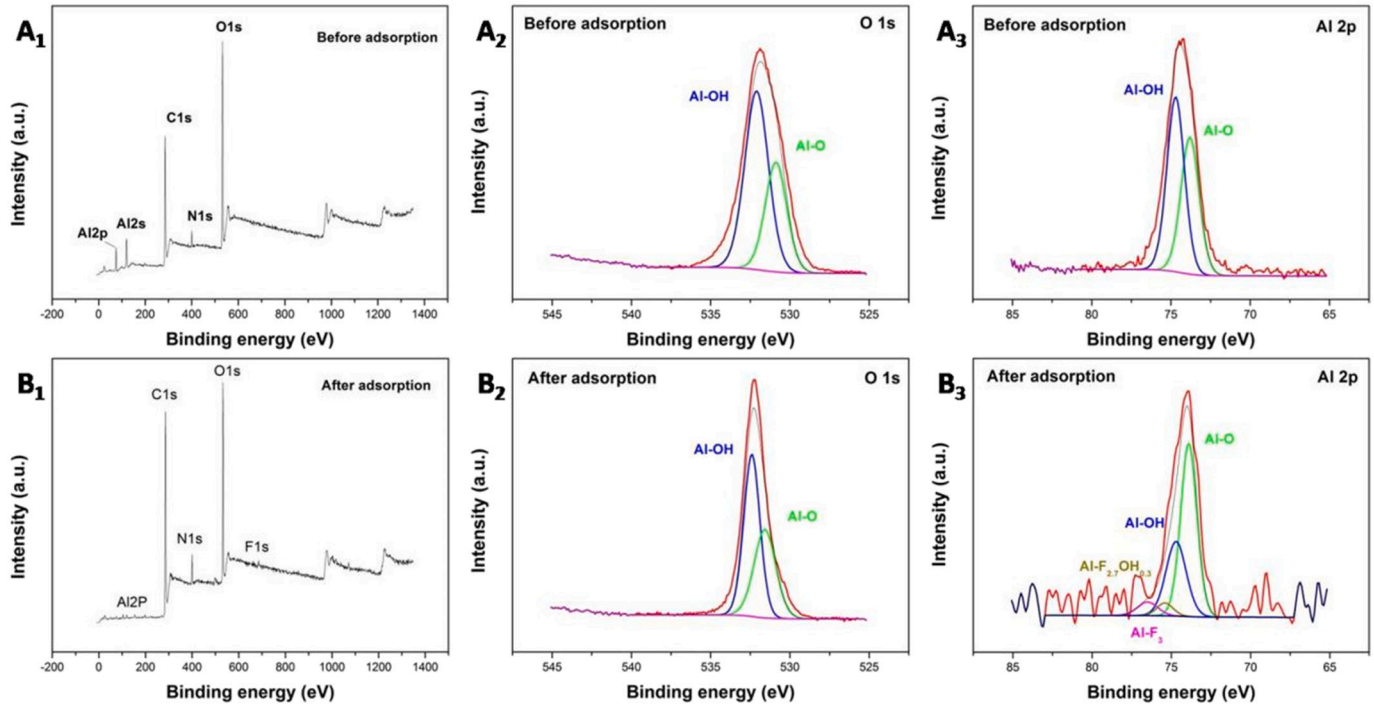

Fig. 7. The XPS analysis of the wide scans (A_1 and B_1), O 1s (A_2 and B_2) and Al 2p (A_3 and A3) before and after adsorption.

Table 3
Element surface compositions of the PUF-Al_2O_3 before and after adsorption by XPS.

Membrane	Element (at. %)				
	C	O	N	Al	F
Before adsorption	52.93	30.49	4.15	12.43	0
After adsorption	70.44	22.36	5.89	0.76	0.55

between 5.5 and 6.5 in the adsorption process:

$$Al_2O_3 - OH + F^- \leftrightarrow Al_2O_3 - F + OH^- \quad (9)$$

$$Al_2O_3 - OH + F^- \leftrightarrow Al_2O_3 - O - H\cdots F^- \quad (10)$$

$$Al_2O_3 - OH + H^+ \leftrightarrow Al_2O_3 - OH_2^+ \quad (11)$$

$$Al_2O_3 - OH_2^+ + F^- \leftrightarrow Al_2O_3 - OH_2^+ \bullet F^- \quad (12)$$

$$Al_2O_3 - OH_2^+ + F^- \leftrightarrow Al_2O_3 - F + H_2O \quad (13)$$

4. Conclusion

A novel PUF-Al_2O_3 composite foam was successfully prepared by employing a sample of dopamine hydrochloride as the underwater adhesive synergistic activated nano-Al_2O_3 loaded onto PUF open cell foam for removing fluoride from water. The PUF-Al_2O_3 retained persistent fluoride ion adsorption capacity, while the composite foam demonstrated excellent regeneration performance after 5 cycles. Highlighted in this study was the stability of nanoparticles when introduced into the PUF. The primary adsorption fluorine ion mechanism of the PUF-Al_2O_3 composite foam was analyzed using ion exchange. Finally, this research provides a new preparative technique that is potentially ideal for nano-adsorbent regeneration and recycling, especially for low concentration fluorine removal. Modern practical applications for treating fluorine-containing water are now possible due to the research carried out here.

Declaration of competing interest

The authors declare that they have no known competing financial interests or personal relationships that could have appeared to influence the work reported in this paper.

Acknowledgements

This research was supported by the Research Project of Tianjin Education Commission (No. 2019KJ097), Tianjin Municipal Science and Technology Bureau of China (Project No. 18PTZWHZ00140, 20JCZDJC00380, 20JCYBJC00560) and TG Hilyte Environment Technology (Beijing) Co., LTD. (Project No. M-P-0-181001-001).

References

[1] U. Kumari, S.K. Behera, B.C. Meikap, A novel acid modified alumina adsorbent with enhanced defluoridation property: kinetics, isotherm study and applicability on industrial wastewater, J. Hazard. Mater. 365 (2019) 868–882, https://doi.org/10.1016/j.jhazmat.2018.11.064.
[2] G.J. Millar, S.J. Couperthwaite, L.A. Dawes, S. Thompson, J. Spencer, Activated alumina for the removal of fluoride ions from high alkalinity groundwater: new insights from equilibrium and column studies with multicomponent solutions, Sep. Purif. Technol. 187 (2017) 14–24, https://doi.org/10.1016/j.seppur.2017.06.042.
[3] Q. Dong, D.X. Yang, L. Luo, Q. He, F.S. Cai, S. Cheng, Y. Chen, Engineering porous biochar for capacitive fluorine removal, Sep. Purif. Technol. 257 (2021), 117932, https://doi.org/10.1016/j.seppur.2020.117932.
[4] X. Wang, G. Zhang, H.C. Lan, R.P. Liu, H.J. Liu, J.H. Qu, Preparation of hollow fe-Al binary metal oxyhydroxide for efficient aqueous fluoride removal, Colloids Surf. A Physicochem. Eng. Asp. 520 (2017) 580–589, https://doi.org/10.1016/j.colsurfa.2017.02.017.
[5] World Health Organization, Guidelines for Drinking-Water Quality: Fourth Edition Incorporating the First Addendum, World Health Organization, Geneva, 2017.
[6] S. Dubey, M. Grawal, A.B. Gupta, Advances in coagulation technique for treatment of fluoride-contaminated water: a critical review, Rev. Chem. Eng. 35 (2018) 109–137, https://doi.org/10.1515/revce-2017-0043.
[7] J.S. He, A.A. Cui, F. Ni, S.H. Deng, F. Shen, C. Song, L. Lou, D. Tian, C.R. Huang, L. L. Long, In situ-generated yttrium-based nanoparticle/polyethersulfone composite adsorptive membranes: development, characterization, and membrane formation mechanism, J. Colloid Interf. Sci. 536 (2019) 710–721, https://doi.org/10.1016/j.jcis.2018.10.064.
[8] J.G. Cai, Y.Y. Zhang, B.C. Pan, W.M. Zhang, L. Lv, Q.X. Zhang, Efficient defluoridation of water using reusable nanocrystalline layered double hydroxides

impregnated polystyrene anion exchanger, Water Res. 102 (2016) 109–116, https://doi.org/10.1016/j.watres.2016.06.030.
[9] Y.X. Zhang, Y. Jia, Fluoride adsorption on manganese carbonate: ion-exchange based on the surface carbonate-like groups and hydroxyl groups, J. Colloid Interface Sci. 510 (2018) 407–417, https://doi.org/10.1016/j.jcis.2017.09.090.
[10] T. Robshaw, S. Tukra, D.B. Hammond, G.J. Leggett, M.D. Ogden, Highly efficient fluoride extraction from simulant leachate of spent potlining via La-loaded chelating resin. An equilibrium study, J. Hazard. Mater. 361 (2019) 200–209, https://doi.org/10.1016/j.jhazmat.2018.07.036.
[11] L.M. Camacho, A. Torres, D. Saha, S. Deng, Adsorption equilibrium and kinetics of fluoride on sol-gel-derived activated alumina adsorbents, J. Colloid Interface Sci. 349 (2010) 307–313, https://doi.org/10.1016/j.jcis.2010.05.066.
[12] M. Sharma, D. Mondal, N. Singh, K. Upadhyay, A. Rawat, R.V. Devkar, R. A. Sequeira, K. Prasad, Seaweed-derived nontoxic functionalized graphene sheets as sustainable materials for the efficient removal of fluoride from high fluoride containing drinking water, ACS Sustain. Chem. Eng. 5 (2017) 3488–3498, https://doi.org/10.1021/acssuschemeng.7b00198.
[13] Z.C. Yu, C.H. Xu, K.K. Yuan, X.Z. Gan, C. Feng, X.Q. Wang, L.Y. Zhu, G.H. Zhang, D. Xu, Characterization and adsorption mechanism of ZrO2 mesoporous fibers for health-hazardous fluoride removal, J. Hazard. Mater. 346 (2018) 82–92.
[14] A. Dhillon, B.L. Sapna, D. Choudhary, S. Kumar, Prasad, excellent disinfection and fluoride removal using bifunctional nanocomposite, Chem. Eng. J. 337 (2018) 193–200, https://doi.org/10.1016/j.cej.2017.12.030.
[15] U. Kumari, S.K. Behera, H. Siddiqi, B.C. Meikap, Facile method to synthesize efficient adsorbent from alumina by nitric acid activation: batch scale defluoridation, kinetics, isotherm studies and implementation on industrial wastewater treatment, J. Hazard. Mater. 381 (2020), 120917, https://doi.org/10.1016/j.jhazmat.2019.120917.
[16] S. Ayoob, A.K. Gupta, P.B. Bhakat, V.T. Bhat, Investigations on the kinetics and mechanisms of sorptive removal of fluoride from water using alumina cement granules, Chem. Eng. J. 140 (2008) 6–14, https://doi.org/10.1016/j.cej.2007.08.029.
[17] H. Wang, Q.M. Feng, K. Liu, Z.S. Li, X.K. Tang, G.Z. Li, Highly efficient fluoride adsorption from aqueous solution by nepheline prepared from kaolinite through alkali-hydrothermal process, J. Environ. Manag. 196 (2017) 72–79, https://doi.org/10.1016/j.jenvman.2017.03.015.
[18] W. Tao, H. Zhong, X.B. Pan, P. Wang, H.Y. Wang, L. Huang, Removal of fluoride from wastewater solution using ce-AlOOH with oxalic acid as modification, J. Hazard. Mater. 384 (2020), 121373, https://doi.org/10.1016/j.jhazmat.2019.121373.
[19] E. Kumar, A. Bhatnagar, U. Kumar, M. Sillanpää, Defluoridation from aqueous solutions by nano-alumina: characterization and sorption studies, J. Hazard. Mater. 186 (2011) 1042–1049, https://doi.org/10.1016/j.jhazmat.2010.11.102.
[20] L.D. Hafshejani, S. Tangsir, E. Daneshvar, M. Maljanen, A. Lähde, J. Jokiniemi, M. Naushad, A. Bhatnagar, Optimization of fluoride removal from aqueous solution by Al2O3 nanoparticles, J. Mol. Liq. 238 (2017) 254–262, https://doi.org/10.1016/j.molliq.2017.04.104.
[21] K. Yang, Y.F. Li, Z.L. Tian, K. Peng, Y.Q. Lai, Removal of fluoride ions from ZnSO4 electrolyte by amorphous porous Al2O3 microfiber clusters: adsorption performance and mechanism, Hydrometallurgy 197 (2020), 105455, https://doi.org/10.1016/j.hydromet.2020.105455.
[22] S.Y. Lu, G. Meng, C. Wang, H. Chen, Photocatalytic inactivation of airborne bacteria in a polyurethane foam reactor loaded with a hybrid of MXene and anatase TiO2 exposing 001 facets, Chem. Eng. J. 404 (2021), 126526, https://doi.org/10.1016/j.cej.2020.126526.
[23] C. Zhang, Y. Li, H.C. Shen, D.M. Shuai, Simultaneous coupling of photocatalytic and biological processes: a promising synergistic alternative for enhancing decontamination of recalcitrant compounds in water, Chem. Eng. J. 403 (2021), 126365, https://doi.org/10.1016/j.cej.2020.126365.
[24] Y.H. Zhao, Y. Wu, L. Wang, M.M. Zhang, X. Chen, M.J. Liu, J. Fan, J.Q. Liu, F. Zhou, Z.K. Wang, Bio-inspired reversible underwater adhesive, Nat. Commun. 8 (2017) 2218, https://doi.org/10.1038/s41467-017-02387-2.
[25] J.Q. Wang, Z.Y. Wu, T.T. Li, J.R. Ye, L.Q. Shen, Z. She, F. Liu, Catalytic PVDF membrane for continuous reduction and separation of p-nitrophenol and methylene blue in emulsified oil solution, Chem. Eng. J. 334 (2018) 579–586, https://doi.org/10.1016/j.cej.2017.10.055.
[26] Q. Du, G.X. Li, S.S. Zhang, J.P. Song, Y. Zhao, F. Yang, High-dispersion zero-valent iron particles stabilized by artificial humic acid for lead ion removal, J. Hazard. Mater. 383 (2020), 121170, https://doi.org/10.1016/j.jhazmat.2019.121170.
[27] Q.L. Cui, J.L. Xu, W. Wang, L.S. Tan, Y.X. Cui, T.T. Wang, G.L. Li, D. She, J. Y. Zheng, Phosphorus recovery by core-shell γ-Al2O3/Fe3O4 biochar composite from aqueous phosphate solutions, Sci. Total Environ. 729 (2020), 138892, https://doi.org/10.1016/j.scitotenv.2020.138892.
[28] K. Yang, Y.F. Li, Z.J. Zhao, Z.L. Tian, Y.Q. Lai, Amorphous porous layered-Al2O3 derived from Al fu MOFs as an adsorbent for removing fluorine ions in industrial ZnSO4 solution, Chem. Eng. Res. Des. 153 (2020) 562–571, https://doi.org/10.1016/j.cherd.2019.11.019.
[29] Z. Wang, K.Y. Ma, Y.F. Zhang, X.B. Zhang, H.H. Ngo, J.Q. Meng, L.Z. Du, High internal phase emulsion hierarchical porous polymer grafting polyol compounds for boron removal, J. Water Process Eng. 41 (2021), 102025, https://doi.org/10.1016/j.jwpe.2021.102025.
[30] Z. Wang, P. Wang, J.J. Cao, Y.F. Zhang, B.W. Cheng, J.Q. Meng, A novel mixed matrix membrane allowing for flow-through removal of boron, Chem. Eng. J. 308 (2017) 557–567, https://doi.org/10.1016/j.cej.2016.09.094.
[31] W.M. Shi, Y.W. Fu, W. Jiang, Y.Y. Ye, J.X. Kang, D.Q. Liu, Y.Z. Ren, D.S. Li, C. G. Luo, Z. Xu, Enhanced phosphate removal by zeolite loaded with Mg–Al–La ternary (hydr) oxides from aqueous solutions: performance and mechanism, Chem. Eng. J. 357 (2019) 33–44, https://doi.org/10.1016/j.cej.2018.08.003.
[32] A.K.D.V.K. Wimalasiri, M.S. Fernando, G.R. Williams, D.P. Dissanayake, K.M.N. de Silva, R.M. de Silva, Microwave assisted accelerated fluoride adsorption by porous nanohydroxyapatite, Mater. Chem. Phys. 257 (2021), 123712, https://doi.org/10.1016/j.matchemphys.2020.123712.
[33] R.L. Tseng, P.H. Wu, F.C. Wu, R.S. Juang, A convenient method to determine kinetic parameters of adsorption processes by nonlinear regression of pseudo-nth-order equation, Chem. Eng. J. 237 (2014) 153–161, https://doi.org/10.1016/j.cej.2013.10.013.
[34] J. Zhou, W.K. Zhu, J. Yu, H.P. Zhang, Y.D. Zhang, X.Y. Lin, X.G. Luo, Highly selective and efficient removal of fluoride from ground water by layered Al-zr-La tri-metal hydroxide, Appl. Surf. Sci. 435 (2018) 920–927, https://doi.org/10.1016/j.apsusc.2017.11.108.
[35] L. Huang, Z.H. Yang, Y.J. He, L.Y. Chai, W.C. Yang, H.Y. Deng, H.Y. Wang, Y. S. Chen, J. Crittenden, Adsorption mechanism for removing different species of fluoride by designing of core-shell boehmite, J. Hazard. Mater. 394 (2020), 122555, https://doi.org/10.1016/j.jhazmat.2020.122555.
[36] F.C. Wu, R.L. Tseng, R.S. Juang, Characteristics of elovich equation used for the analysis of adsorption kinetics in dye-chitosan systems, Chem. Eng. J. 150 (2009) 366–373, https://doi.org/10.1016/j.cej.2009.01.014.
[37] Z.X. Jin, X.X. Wang, Y.B. Sun, Y.J. Ai, X.K. Wang, Adsorption of 4-n-nonylphenol and bisphenol-a on magnetic reduced graphene oxides: a combined experimental and theoretical studies, Environ. Sci. Technol. 49 (2015) 9168–9175, https://doi.org/10.1021/acs.est.5b02022.
[38] J.R. Lindsay, H.J. Rose, W.E. Swartz, P.H. Watts, K.A. Rayburn, X-ray photoelectron spectra of aluminum oxides: structural effects on the “Chemical shift”, Appl. Spectrosc. 27 (1973) 1–5, https://doi.org/10.1366/000370273774333876.
[39] B.R. Strohmeier, Surface characterization of aluminum foil annealed in the presence of ammonium fluoborite, Appl. Surf. Sci. 40 (1989) 249–263, https://doi.org/10.1016/0169-4332(89)90009-3.
[40] A. Hess, E. Kemnitz, A. Lippitz, W.E.S. Unger, D.H. Menz, ESCA, XRD and IR characterization of aluminum oxide, hydroxyfluoride, and fluoride surfaces in correlation with their catalytic activity in heterogeneous halogen exchange reactions, J. Catal. 148 (1994) 270–280, https://doi.org/10.1006/jcat.1994.1208.
[41] Y.X. Zhang, Y. Jia, Fluoride adsorption onto amorphous aluminum hydroxide: roles of the surface acetate anions, J. Colloid Interface Sci. 483 (2016) 295–306.
[42] Y.L. Guo, X. Xu, Y.N. Shang, B.Y. Gao, L. Zhang, Q.Y. Yue, Q. Li, Z.H. Wang, Multiple bimetallic (Al-La or fe-La) hydroxides embedded in cellulose/graphene hybrids for uptake of fluoride with phosphate surroundings, J. Hazard. Mater. 379 (2019), 120634, https://doi.org/10.1016/j.jhazmat.2019.05.027.